Cell remote mechanics regulates large-spatial matrix modeling with dynamic simulations

Mingxing Ouyang[1,#,*], Yanling Hu[1,#], Weihui Chen[1], Hui Li[1], Yingbo Ji[1], Baohua Ji[2], Bing Bu[1,*],

Linhong Deng[1,*]

[1]Institute of Biomedical Engineering and Health Sciences, School of Medical and Health Engineering & School of Pharmacy, Changzhou University, Changzhou, 213164 China

[2]Institute of Applied Mechanics, Department of Engineering Mechanics, Zhejiang University, Hangzhou, 310027 China

[#]Shared first authorships

[*]Corresponding authors:

Dr. Mingxing Ouyang

Professor at Institute of Biomedical Engineering and Health Sciences,
School of Medical and Health Engineering, Changzhou University
1 Gehu Rd, Wujin District, Changzhou, 213164 China
Email: mxouyang@cczu.edu.cn

Dr. Linhong Deng

Fellow of AIBME, Cheung Kung Distinguished Professor
Founding Director Institute of Biomedical Engineering and Health Sciences,
School of Medical and Health Engineering, Changzhou University
1 Gehu Rd, Wujin District, Changzhou, Jiangsu Province 213164 China
Email: dlh@cczu.edu.cn

Dr. Bing Bu
Lecturer at Institute of Biomedical Engineering and Health Sciences,
School of Medical and Health Engineering, Changzhou University
1 Gehu Rd, Wujin District, Changzhou, 213164 China
Email: bubing@cczu.edu.cn

Running title: Dynamic biomechanics-induced large ECM modeling

Abstract

Tissues and organs often have specific structures or shapes, which developmental process is coordinated by cells and extracellular matrix modeling. The biomechanical aspect how cells and matrix manage large-spatial constructions for tissue morphogenesis or bioengineering has got increasing attentions, while long-range mechanical communications by cells provide certain insights. Previous work has demonstrated the capability of cells in remodeling matrix structures in distance, however, which biophysical mechanistic studies are still pretty conditional. Here, we investigated the underlying dynamic mechanism of collagen I (COL) fibrillary modeling remotely induced by cell traction force, and the involved cellular mechano-signaling. The research designs were based on large arrays of cell clusters, and with incorporated dynamic tractions, the Molecular Dynamics simulations yielded highly matching outcomes with observed COL fiber clustering in experiments based on large-spatial square, parallelogram, and random-style arrays of cell clusters. The further designed single polygons with variable geometries from triangles to hexagons resulted in predicted structures with assembled COL fibers, which space balance was not maintained when introducing additional contraction at their geometrical centers. The cell cytoskeletal integrity (actin filaments, microtubules), actomyosin contractions, and endoplasmic reticulum calcium channels were essential for the remote fiber inductions, whereas membrane mechanosensitive integrin β1 or Piezo1 alone was less critical in fiber assembly. This work provided new mechanistic insights with dynamic and spatial factors on remote induction of matrix modeling by cells at tissue scale, and the involved cellular mechanism. The assembled biomechanical scaffolds based on pre-designs may lead to applications in tissue engineering.

Introduction

Tissues and organs in the body have specific structures or shapes, which developmental process is coordinated by cells and ECM modeling[1; 2]. Abnormal ECM modeling is often a sign for disorders, such as fibrosis in liver and lung, cartilage degradation in joints, and ECM-associated genetic diseases[3]. Several studies demonstrated tumor cells able to reconstruct ECM environments in facilitating the metastasis[4; 5; 6]. Cells also show the capability in remote ECM modeling, for example, two explanted fibroblast tissues could build fibers within 1.5-4 cm separation on the collagen hydrogel[7; 8]. Hence, cells can format ECM structure which in return mediates the physiological outcomes of cells and tissues. Beside the chemical cues, the biomechanical aspect how cells and ECM coordinate at the large-spatial scale during morphogenesis and for tissue engineering has been an interesting topic to explore.

Cell mechanical communications are recognized from in vitro and in vivo studies[9; 10]. Some different from traditional chemical cues, mechanical communications between cells show the features with long-range or large-spatial transmission, precise direction, and functional outcomes at tissue scale. For example, cells are able to sense the positions of neighboring cells through compliant substrates[11; 12]. Long-range force enables assembly of mammary tissue patterns and collagen fibrillary remodeling[13; 14]. Cardiomyocytes achieved similar beating frequency when seeding on elastic substrate[15; 16]. During *Xenopus* embryonic development, the cell cluster of neuronal crest moves collectively to the destination with supracellular contraction at the rear to assist directional migration[17; 18]. These increasing evidences have supported distant mechanical communication as a common nature of cells.

The cellular mechanism on mechanical communications has also been under study. As shown from recent work including ours, cells have the capability to sense the traction force or substrate

deformation transmitted from neighboring cells or induced by external probe, which provides a bridge in understanding cell-cell distance interactions[19; 20]. At the molecular level, the mechanosensitive receptor integrin and ion channel Piezo display importance in remote attractions between two types of cells[21; 22]. The calcium channels on endoplasmic reticulum (ER) are indispensable for cell distant mechanical interactions[23]. There is also long-range force transmission through cell-cell junctions during the collective migration of epithelial sheet[24; 25]. So far, some important mechanism and signals have been identified for the mechanical communications, whereas the general map at this aspect is still limited.

There is underlying physical mechanism to transmit mechanics between cells for long-range interactions. Two pathways have been shown up: mechanical transmission through the nonlinear elastic hydrogel such as type I collagen (COL), or via cell-cell junctions along the epithelial layer. Experimental results together with computational modeling demonstrated that fibrous biological gel can facilitate the efficient transmission of traction force for intercellular mechanical communications[26; 27; 28]. Recent evidence shows that cells-reorganized fiber bundles bear the major tensile force to guide cell distant interaction and correlated migration[29]. Breast cancer cells can orient the COL fibers to direct the metastatic intravasation[5]. One earlier study suggested that the strain stiffening of fibrous gel isn't sufficient to support such long-distance for cell sensation[30], and later study provided insight that cells are capable of mechanosensing the traction force transmitted distantly from other cells[19].

As one interesting observation, cells are able to reconstruct the COL gel to generate fibrous bundles[8; 31], which biophysical mechanism has attracted research attentions. Harris lab first demonstrated physical force from tissues able to rearrange COL patterns with long-range order[32]. A later study confirmed the local movements of COL driven by fibroblast contractions leading to

4

the fibrillary organization[33]. In recent decade, more mechanistic work has emerged on the cells-driven fibrous morphogenesis. Finite element (FE) simulations predicted the alignment of COL gel induced by long-range biomechanical transmission, although the results were conditional with anisotropic cell shape and within cell pair[34; 35]. FE simulations combined with fibrous continuum modeling further yielded the measurements of cell traction force propagation[36]. By application of optical tweezers to pull beads on the COL hydrogel, Han *et al.* revealed the long-range stiffness gradients surrounding the cell[37]. Chen and Baker designed synthetic fibrous materials with controllable biomechanical architectures, and observed cell contraction-mediated alignment of fibers[38; 39]. In mimicking in vivo condition, experimental stretch or fluidic shear stress is also able to align long-range order of extracellular matrix (ECM)[40; 41]. In general, how to understand cells-induced ECM remodeling at large-spatial or tissue scale is still challenging.

Apparently, cells conduct the work in remodeling ECM microenvironment in physiology and pathology, which intracellular signaling is to be understood. Cancer-associated fibroblasts (CAFs) can induce COL cross-link switch, and align fibrous COL or fibronectin to promote fibroblast long-range order or direct cancer cell migration[4; 6; 42]. Early-stage cancer cell spheroids embedded into COL containing fibroblasts generated force for fibers alignment and CAFs induction[43]. Our work also showed that motile kidney epithelial cells (MDCK) can actively recruit soluble ECM from the medium to assemble base membrane or COL architectures in directing spherical or tubular tissue formations[44; 45]. The cell signals of integrin, RhoA, and actomyosin contraction show importance in cells-mediated ECM remodeling[4; 46]. However, the fundamental molecular mechanism in cells remotely driving the modeling is largely unknown.

In this work, we tried to study the COL fibrillary remodeling induced by cell long-range traction force, as well as the involved mechano-signaling mechanism in cells. The research designs were

based on large-spatial arrays of cell clusters and incorporated an important feature with dynamic traction force in simulations. This helped overcome the limitations of previously conditional studies, for example, the objective of single or a few cells/clusters, a demand for polarize cell shape, or static traction force[47]. In previous work, we observed the traction force from live cells is a dynamic factor instead of static through the hydrogel, which was derived from the highly motile cell clusters under constantly rotating [13; 44], as reported by Bissel group as well[48]. In this work with incorporated dynamic tractions, the simulations with Molecular Dynamics yielded highly matching outcomes with the observed COL fiber bands from the experiments, which didn't have conditional spatial-scale limitation. The designed single polygons with variable geometries led to well predicted structures with assembled COL fibers, which balance was not maintained when introducing additional contraction at the geometrical centers. The cell cytoskeletal integrity, actomyosin contractions, and ER calcium channels were essential for the remote induction of COL fibers, whereas the role of membrane mechanosensitive integrin β1 or Piezo1 alone was less critical. This work provided new mechanistic insights on the remote induction of ECM modeling by cells, as well as the relevant cellular molecular mechanism. The assembled scaffolds based on pre-designs may also lead to promising application in tissue engineering.

Materials and Methods

Cell Culture and siRNA transfection

Rat airway smooth muscle (ASM) cells were isolated from the tracheal tissue of 6-8-week old female Sprague Dawley rats as described previously[49]. The cells were cultured in low sugar DMEM (Invitrogen) supplemented with 10% fetal bovine serum (GIBCO) and

6

penicillin/Streptomycin antibiotics (GIBCO). The cells used in the experiments were generally maintained within 10 passages.

To perform siRNA transfections, ASM cells were seeded into 6-well plate at ~40% density, and the next day, rat ITGB1 siRNA (Thermo), Piezo1 siRNA (Horizon Discovery), or control siRNA (50 nM in 2 mL medium) was transfected into the cells by using 5 µL Lipofectamine 3000™ reagent. After incubation for about 8 h, changed the medium and waited for 48~72 h before further experiments.

Preparation of PDMS molds

The micro-patterned arrays of cell clusters were prepared according to the method derived from our previous work[13], but with more variably geometrical distributions. Basically, we used the software AutoCAD to design the arrays of circle distributions, which circles were set as 200 µm in both diameter and depth, and 600-800 µm in mutual spatial separation. The parameters for different geometrical patterns are listed in Table 1. The silicon wafers printed with the designs were manufactured by Suzhou MicroFlu Technology Co., Ltd. and In Situ Co., Ltd.

Table 1. The parameters for variable geometric patterns.

Distribution geometries of circles	Parallelogram Arrays	Square Arrays	Random Arrays	Triangle	Parallelogram	Square	Pentagon	Hexagon	Triangle (+)	Parallelogram (+)	Square (+)	Pentagon (+)	Hexagon (+)
Geometric patterns (circles with 200 µm in diameter)													
Mutual space separation (µm)	800	800	/	600	600	600	600	600	600 (side)	600 (side)	600 (side)	600 (side)	600 (side)

To fabricate the polydimethylsiloxane (PDMS) molds, the two liquid components from the Sylgard 184 Kit (Dow Corning) were mixed at a mass ratio of 10:1 (base to catalyst 87-RC), and poured onto the silicon wafer after extraction of air bubbles by vacuum, then cured at 80°C for over 4 h and left at room temperature overnight. The solidified PDMS was carefully peeled off

from the wafer, and further cut into small pieces (~ 1x1 cm) to adapt the next experimental utility. The prepared PDMS molds were soaked in 75% ethanol for disinfection, and exposed to UV light for several hours in the cell culture hood before each experiment.

Expression and purification of EGFP-CNA35 protein

The pET28a-EGFP-CNA35 DNA construct purchased from Addgene was described before[50]. The procedures for expression and purification of EGFP-CNA35 protein were introduced in our recent work[19]. In brief, the DNA plasmid was transformed into BL21 (DE3) competent bacteria, and when culturing in the Lysogeny Broth (LB) medium, the protein expression was induced by isopropyl β-D-1-thiogalactopyranoside (IPTG) at room temperature. The precipitated bacteria were lysed with B-PER lysate solution (Thermo Scientific), and HisPur Ni-NTA agarose beads were added to pull down the 6xHis-tagged protein. The concentration of purified protein was measured by Branford protein assay kit (Thermo), and protein aliquots were stored at -80°C.

PDMS mold-printing onto agarose gel, and cell cluster culture

First, to prepare cell clusters on micro-patterned agarose gel. Agarose solution (20 g/L) was made by dissolving 2 g agarose (Thermo) in 100 mL sterile Phosphate-Buffered Saline (PBS) by microwaving, and ~150 μL agarose solution was dropped onto the glass-bottom dish. The sterilized PDMS mold was placed onto the solution, and slightly pressed downward. After solidification at room temperature, carefully peeled off the mold without disruption of the printed patterns on agarose gel. 200 μL suspension of ASM cells in medium (~1.2 x 10^6 cells/mL) was added onto the agarose gel, and after 10-15 min waiting for cells to settle down into the pattern areas, absorbed the additional medium away and washed the patterned regions once or twice with

culture medium carefully. Then, cells were generally filled into the circular caves (200 μm in depth) without much left on other areas (cells are non-adhesive on agarose gel).

Second, to cover the cell clusters with fluorescent COL (Cultrex 3-D Culture Matrix Rat Collagen I) hydrogel. The preparation of COL solution was carried out on ice: completely mixed the rat tail COL solution (4 mg/ml) with purified EGFP-CNA35 protein (diluted to 1 mg/ml in advance) at the volume ratio of 5:1, and waited for about 15 minutes; afterwards, added neutralizing solution at 1:9 volume ratio of the COL one, and further diluted the COL to final 1 mg/ml (or other alternative concentration) with PBS. Then added the mixed COL solution (300-400 μL) onto the patterned cells-containing agarose gel, and tried to spread the COL liquid across the glass-bottom surface of the dish in addressing none adhesive COL gel onto agarose. Then placed the assembled cell samples in the culture incubator at 37°C for 15~20 min, and after gel, added 2 ml of regular culture medium into the dish. In this way, the cell clusters were generally embedded into COL while underneath the gel layer.

Cell cluster cultures along with inhibitor applications

Before detached for generating cell cluster arrays, ASM cells cultured in six-well plates (NEST) were pre-incubated with the inhibitors for 1~2 h, and the solvent DMSO (Beyotime) was used as control. After cell clusters were sandwiched between COL and agarose gels, the culture medium containing the same inhibitor was added back. To enhance the medium diffusion with inhibitor through the hydrogel, a small hole was created at the edge of the gel with a fine needle without disturbing the cell mass. After culture for 24 hours, 1 mL more medium with the same inhibitor was further supplemented to the culture in considering the inhibitor stability at 37°C. The formation of COL fiber bands and cell migration were recorded under microscopy.

The applied inhibitors in the experiments were mostly purchased from Sigma, including 2-Amino-ethoxydiphenyl borate (2-APB, an IP_3R calcium channel inhibitor with cell permeability, 20 µM), Nifedipine (membrane L-type calcium channel inhibitor, 20 µM), Lanthanoum(III) chloride ($LaCl_3$, SOC calcium channel inhibitor, 100 µM), Nocodazole (microtubule de-polymerizing agent, 1 µM), Blebbistatin (myosin II ATPase inhibitor, 40 µM), Cytochalasin D (CytoD, actin polymerization inhibitor, 1 µM), ML-7 (MLCK inhibitor, 40 µM), NSC23766 (Rac1 activation inhibitor, 100 µM), and Latrunculin A (LatA, microfilament polymerization inhibitor, 237 nM). Y27632 (ROCK inhibitor, 40 µM) was from MedChemExpress, and Thapsigargin (ER SERCA pump inhibitor, 10 µM) from Abcam.

Q-PCR measurements

After ITGB1 or Piezo1 siRNA transfection, the decrease of mRNA expression in ASM cells was evaluated by real-time quantitative PCR (qPCR), which details were described in our recent work[51]. The primer sequences of qPCR derived from others' studies are listed on Table 2[52; 53].

Table 2. The primer sequences of qPCR for measuring ITGB1 and Piezo1 mRNA levels.

Gene Name	Primer(forward)	Primer(reverse)	Company
ITGB1[52]	GAATGGAGTGAATGGGACAGGAG	CAGATGAACTGAAGGACCACCTC	
Piezo1[53]	GACGCCTCACAAGGAAAGC	GGGCAGCATCTATGTCATCC	GENERAL BIOL
GAPDH	AGGTCGGTGTGAACGGATTTG	GGGGTCGTTGATGGCAACA	

Molecular dynamics (MD) simulations of fibers clustering and reconstruction

10

A 2D network model based on MD simulation was introduced to investigate the mechanics of fibers cluster and cell migrations. The collagen fibers were simplified to bonds on a plane, and their crosslinks were set as the nodes between different bonds. The collagen fiber is an isotropic elastic material that has a high modulus in tension and a very low modulus in compression[54]. The bond's tension stiffness was set as 100 times of compression stiffness. The fibers crosslinks may reconstruct under tension or compression. Here we set a reconstruction judgmental condition that bond length change is higher than 50 percent of bond length. The crosslink of this fiber will be reconstructed and this bond length will change from its initial value to its current value. The fibers network under cells region were removed, and cells were shown as a circle with 83 nodes. The Stochastic dynamics (SD) were performed by GROMACS package[55]. The XYZ coordinates of cells nodes and Z coordinates of crosslinks nodes were fixed during simulation. The dynamic contraction of cells was applied as the radius reduction of the cells' circles. The circle radius was reduced by 5% per 50000 simulation steps. The simulation results were analyzed with VMD program[56].

Finite element modeling (FEM) for stress distributions on the hydrogel

The FEM model to investigate the correlation between matrix stress distribution and the fibers network formation has been introduced in our previous studies[19; 57]. The interaction surface of cells and collagen matrix was simplified to an isotropic linear elastic plane surface. The cell region was removed, and cell traction force was applied on the edges of cells' region to mimic the contraction force of cells on the matrix surface. The stress value on the matrix was normalized to reach a relative quantitative analysis and results. The FEM model was solved and visualized by ABAQUS packages.

Live cell imaging, and quantifications of COL fiber intensities

11

The live cell microscopy workstation (Zeiss) was equipped with an X-Y-Z controller system for multi-position imaging, fine auto-focusing function, and a culture chamber loaded on the sample stage to maintain 5% CO_2 and the temperature at 37°C. Most fluorescence imaging experiments were carried out with x5 and x10 objectives under the microscope. One round of the experiments spanned 2-3 days, and the images for fluorescent collagen fibers and cell migrations were taken at different time points as indicated, for example, the initial status, 12, 24, 36, 48 h.

ImageJ was used to quantify the relative fluorescence intensities (FL) of collagen fiber bands in contrast to the close non-fiber areas, as demonstrated in Figure S1. In the procedures, the image was rotated so the COL fibers were displayed in horizontal direction; a rectangular region (ROI) with same size was chosen in covering each COL fiber band and its close area while the fiber band was positioned at the middle of ROI. Averaged fluorescence intensity (FL) was measured from left toward right along the selected rectangular ROI by using the "plot profile" function in ImageJ. The acquired values from each ROI were input into the Excel file, which generated an averaged fluorescence distribution curve along the selected region. Then, the sum (S_{max}) of seven points around the maximum intensity value (three values from the left and another three from the right) was calculated, as well as the sum (S_{min}) of seven values from two ends of the curve (three or four values from each) in representing the low non-fiber intensities. The FL ratio was defined as S_{max} divided by S_{min} (Ratio = S_{max}/S_{min}). Generally, fluorescent COL images were quantified from 4 or 5 time points within 48 h, for instance, 0, 12, 24, 36, 48 h. Statistical comparison was conducted between the initial time point and later ones, which presents the emerging COL fibers induced by cell clusters remotely.

The COL fluorescence curves and graphs of scattering dots were processed by Origin 2020, GraphPad Prism 6, and Excel software. Student's t-test was applied for statistical analysis. *, **,

, * represent 'p value' < 0.05, 0.01, 0.001, 0.0001 for significant difference respectively, while 'NS' for no significant difference.

Results

MD and FEM simulations for COL fiber clustering driven by stress distribution

To study how cell traction force remotely drives clustering of COL fibers on the hydrogel, we built a 2D network model based on MD simulation to investigate the direction and mechanics of fibers cluster (Fig.1A). The collagen fibers were simplified to bonds on a plane, and their crosslinks were set as the nodes between different bonds (Fig.1B). The collagen fiber is an isotropic elastic material that has a high modulus in tension and a very low modulus in compression (Fig.1C) [54].

To investigate how stress distribution regulates fibers clustering, the force direction on each node and maximum shearing stress distribution on matrix was calculated by molecular simulation and FEM respectively. As shown in Fig. 1D, two cells shrunk with dynamic contractions, and fibers cluster between cells from MD simulation. The particle force in MD also revealed similar results (Fig. 1E). Considering the orientation of particle force, the fiber was bearing a pulling force toward the connection line between cells, which would lead to the fibers clustering (seen in Fig. 1D&E). The local maximum shearing stress distribution on matrix was calculated and shown in Fig. 1F, and the black line revealed the direction of first principle stress at local place. The maximum shearing stress has a relatively high value around the connection line of two cells, and this region is consistent with the fibers clustering (Fig. 1F).

For the condition of four cells, fibers clustering formed in relatively closer cell pairs instead of central region of four cells (seen in Fig. 1G). Similar as the condition of two cells, the fiber lines

13

are also in agreement with the first principle stress direction and the particle force distributions (Fig. 1H). The central region has a higher first and second principle stress, but the maximum shearing stress is lower than the connecting lines of cell pairs (Fig. 1I). Taken together, fibers were recruited in the region with higher maximum shearing stress and the orientation of local Maximum Principle Stress.
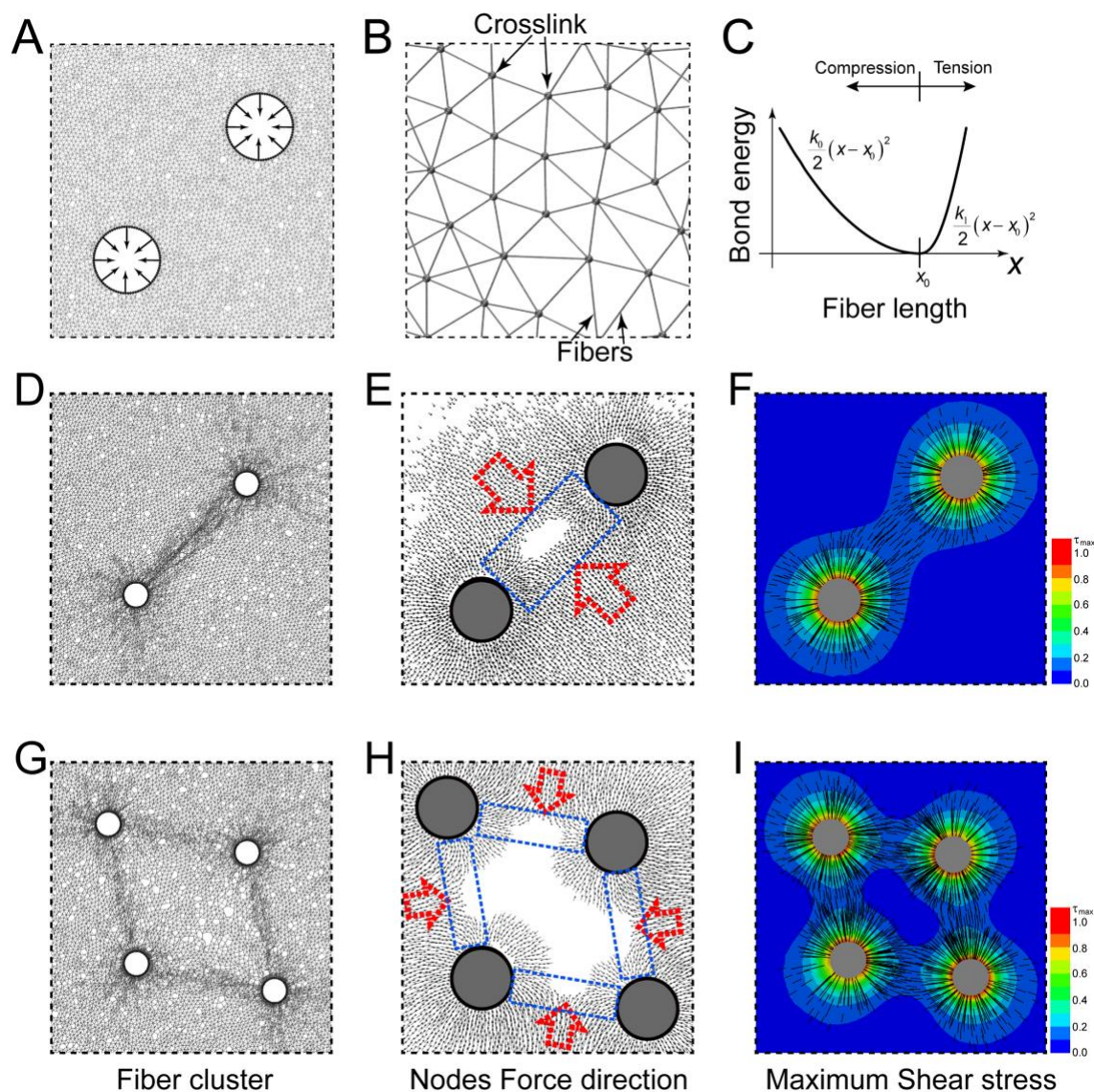

Figure 1. The corresponding relation between fibers clustering and stress distribution.

(A) The molecular dynamics simulation model for fibers clustering. The collagen fibers were

simplified to a bonds network. The contraction of cells was applied on the boundary of the empty regions. **(B)** A detail view of the fibers bonds network. **(C)** The bond energy changes with bond length. When bond was compressed or tensed, the tension spring stiffness is higher than compression spring stiffness. **(D)** Fibers were recruited in the connection line of two cells. **(E)** The particle force distribution and the directions of particle force in two cells by MD simulation. **(F)** The maximum shearing stress distribution on matrix and the directions of first principle stress in two cells condition. **(G)** Fibers were recruited in the connection line of relative close cell pairs in the condition of four cells. **(H)** The particle force distribution and the directions of particle force in four cells by MD simulation. **(I)** The maximum shearing stress distribution on matrix and the directions of first principle stress in four cells condition.

Large-scale COL fiber remodeling induced by geometrical square and parallelogram-arranged cell cluster arrays

The simulated outcomes by Molecular Dynamics (MD) showed fiber cluster occurrence mostly at the sides instead of the diagonal lines, which modeling was based on the dynamic contraction in geometrical square-positioned cell cluster arrays (Fig. 2A). The experimental results were acquired by seeding cell clusters into square or parallelogram arrays covered with fluorescent COL gel (1 mg/ml, labeled with EGFP-CNA35). The images were taken at indicated time points in the next two days. The data showed the emerging square lattices of COL fiber bands, resulting into connection of the cell cluster array (Fig. 2B). More details with the gradual growth of COL fibers in different geometrical arrays were shown in Supplementary Information (Fig. S2A). The fluorescence quantification (Ratio = S_{max}/S_{min}) and intensity distributions indicated the gradual growth of the fibers (Fig. 2C, D). The ratio started at ~1.0 as an initial uniform distribution of fluorescent COL, and reached ~1.2-1.5

15

indicating fiber growth between cell clusters. Fluorescence curves of individual selected ROI regions are presented in Fig. S3. The fiber lattice structure stayed stable through the two-day observations, indicating balanced contraction force through the square array.

We next examined the geometrical parallelogram arrays. MD simulation showed fiber clustering at the sides while less obvious at the diagonal directions (Fig. 2E). When cell clusters were seeded into parallelogram array mode, COL fiber buckling occurred mostly at the sides, resulting into formation of parallelogram lattices (Fig. 2F, more details shown in Fig. S2B). Fluorescence quantification and spatial distributions indicated the gradual accumulations of COL fibers between cell clusters (Fig. 2G, H). As seen at later time (e.g. 36 h) (Fig. S2A, B), certain fiber bands showed up at the diagonal directions in parallelogram and square arrays. This experimental difference from the simulations might be partially due to the changed material property of the hydrogel under remodeling by the cell clusters, which explanation demands further study.

We further applied random-style distributed arrays of cell clusters (mutual spatial separations within 600-1000 μm) to check the simulation and experimental outcomes for fiber growth. The MD simulation well turned out fiber emergences in connecting the cell clusters (Fig. 2I), which dynamic process is shown in Movie 1. Experiments based on random-positioned arrays showed gradual fiber growth between cell clusters, resulting into fiber network formation along with the clusters (less stable structure as well) (Figs. 2J, K and S2C), which indicates the robustness of cell pattern-induced fiber assembly. Therefore, the experimental results of fiber clustering within variable geometries stayed pretty consistent with the MD and FEM simulated outcomes based on dynamic tractions at the large-spatial scale.
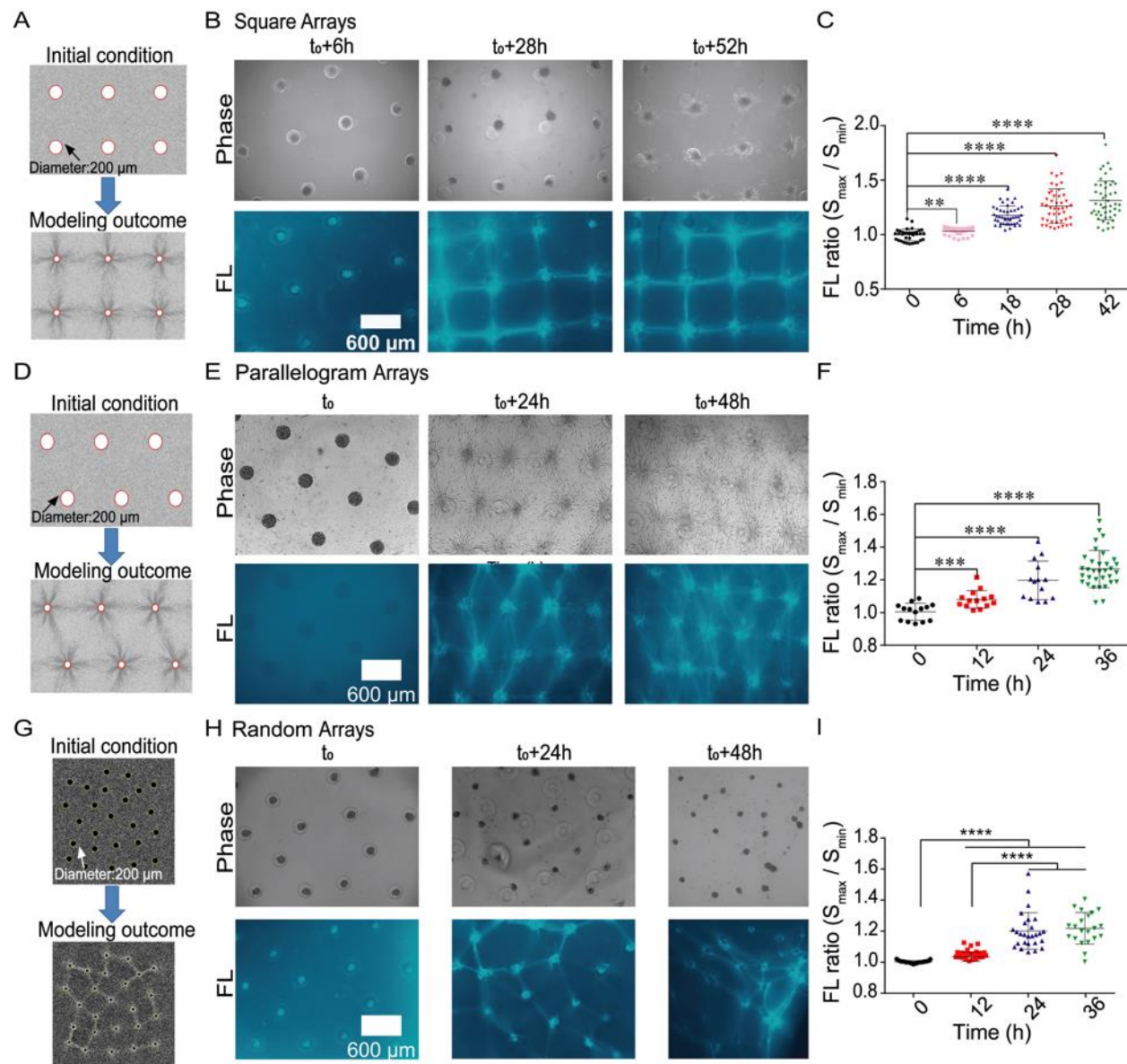
Figure 2. Remote COL fiber inductions by geometrically variable arrays of cell clusters at large-scale. ASM cell clusters were seeded into the designed geometrical arrays with a layer of fluorescent COL hydrogel (1 mg/ml) atop. Images of cells and COL fluorescence were taken at the indicated time within the next two days. **(A)** MD simulated outcome of geometrical square arrays based on dynamic contraction force of cell clusters. **(B)** The emerging COL fiber bands between cell clusters positioned into square arrays at the indicated time. **(C)** Fluorescence (FL) quantification of COL fibers (mean ± S.E.M.) in contrast to the close non-fiber region based on

the ratio calibrations (S_{max}/S_{min}). Each dot in the graph represents a ratio value of one fiber band. **(D)** The spatial distributions of averaged COL fluorescence along with the selected regions (300 μm in width) at the indicated time. The quantification process is described in the Methods. **(E-H)** The MD simulation outcome (**E**), the emerging COL fiber bands (**F**), FL ratio quantifications of COL fiber bands (**G**), and fluorescence distributions along the selected rectangular regions (200 μm in width) (**H**) from the geometrical parallelogram-arranged cell cluster arrays. **(I-K)** The MD simulation outcome (**I**), the emerging COL fiber bands (**J**), FL ratio quantification (**K**) from the geometrical random-style cell cluster arrays. The statistical significance for COL fluorescence between the initial and indicated time points was evaluated by Student's t-test. *, **, ***, **** represent p value < 0.05, 0.01, 0.001, 0.0001, respectively. The presenting methods are similar through the paper.

COL fiber assembly induced in single polygons with diverse geometries

We further designed cell clusters positioned into single polygons including triangles, parallelograms, squares, pentagons, and hexagons (600 μm in mutual separations of the clusters). This provided the chance to assess the robustness of cell contraction-induced COL fiber assembly, and the stability of assembled fiber structures.

When cell clusters were settled down into single triangles, strong COL fibers were shown up at the three sides rapidly (within 12 h), and cells migrated toward each other (Figs. 3A, left). There was also fiber growth between two triangles which had 1000 μm in distance (Fig 3A, left). Fluorescence quantification from a group of samples confirmed fiber assembly from the designed triangles (Fig. 3A, right). In single parallelograms, COL fibers emerged gradually at the four sides along with some shown up at the diagonal lines (600 μm in distance) (Fig. 3B). In single squares,

18

のbioRxiv preprint doi: https://doi.org/10.1101/2022.10.29.514382; this version posted October 31, 2022. The copyright holder for this preprint (which was not certified by peer review) is the author/funder, who has granted bioRxiv a license to display the preprint in perpetuity. It is made available under aCC-BY-NC-ND 4.0 International license.

COL fibers occurred at the four sides, not much at the diagonal direction (848 μm in distance) (Fig. 3C).

When cell clusters were arranged into single pentagons or hexagons, COL fibers were shown up efficiently at the sides, but not at the diagonal lines (Fig. 3D, E). This could be reasonable that the distances between cell clusters at the diagonal directions (~1141, 1039 μm in pentagons, or 1200 μm in hexagons) were much larger that at the sides (600 μm). It is also noted that cells migrated actively toward each other along the sides (Fig. 3D, E). By measuring the area changes within 48 h culture to evaluate the structural stabilities shown in Figure 2, the square arrays were more stable than parallelogram and random-style ones (Fig. 3F, left). The single polygons (Fig. 3A-E) were quite stable (less than 30% shrinking in areas), except triangle ones (~45% shrinking) (Fig. 3F, right). As a demonstration, MD simulation for single parallelogram predicted fiber clustering mostly at the sides, similar to the simulated parallelogram arrays (Fig. 3G), along with FEM simulation of the maximum stress distribution shown in Figure S4A. The more details for fiber inductions from single triangles to hexagons are presented in Figure S4(B-F).

We further examined the complexity-enhanced single polygons and structural stability by introducing additional contraction cluster at the geometrical center of polygons (named as 'polygons(+)'). As show from experiments, when cell clusters were positions within the triangles(+), parallelograms(+), squares(+), pentagons(+), and hexagons(+), COL fibers were still shown up efficiently in one day (Fig. 3H-L). Interestingly, the assembled structures of fibers and cell clusters shrunk in the polygons(+) (>60% reductions in areas), except pentagons(+) with more stability (~40% reduction) within 48 h (Fig. 4M). This suggests the contraction forces within polygons(+) were not as balanced as the simple polygons shown in Figure 3F. As one demonstration, the MD stimulation in hexagon(+) displayed fiber buckling both at the sides and

19

inside the polygon based on dynamic stress distribution (Fig. 4N), along with maximum stress distributions by FEM simulation (Fig. S4G). More details for the single polygons(+) images are presented in Figure S4(H-L). Together, these results from above confirmed the highly consistency of the dynamic simulations and experimental outcomes (especially at the early time stages), and demonstrated the fiber assembly induced by cell traction forces in COL hydrogels.
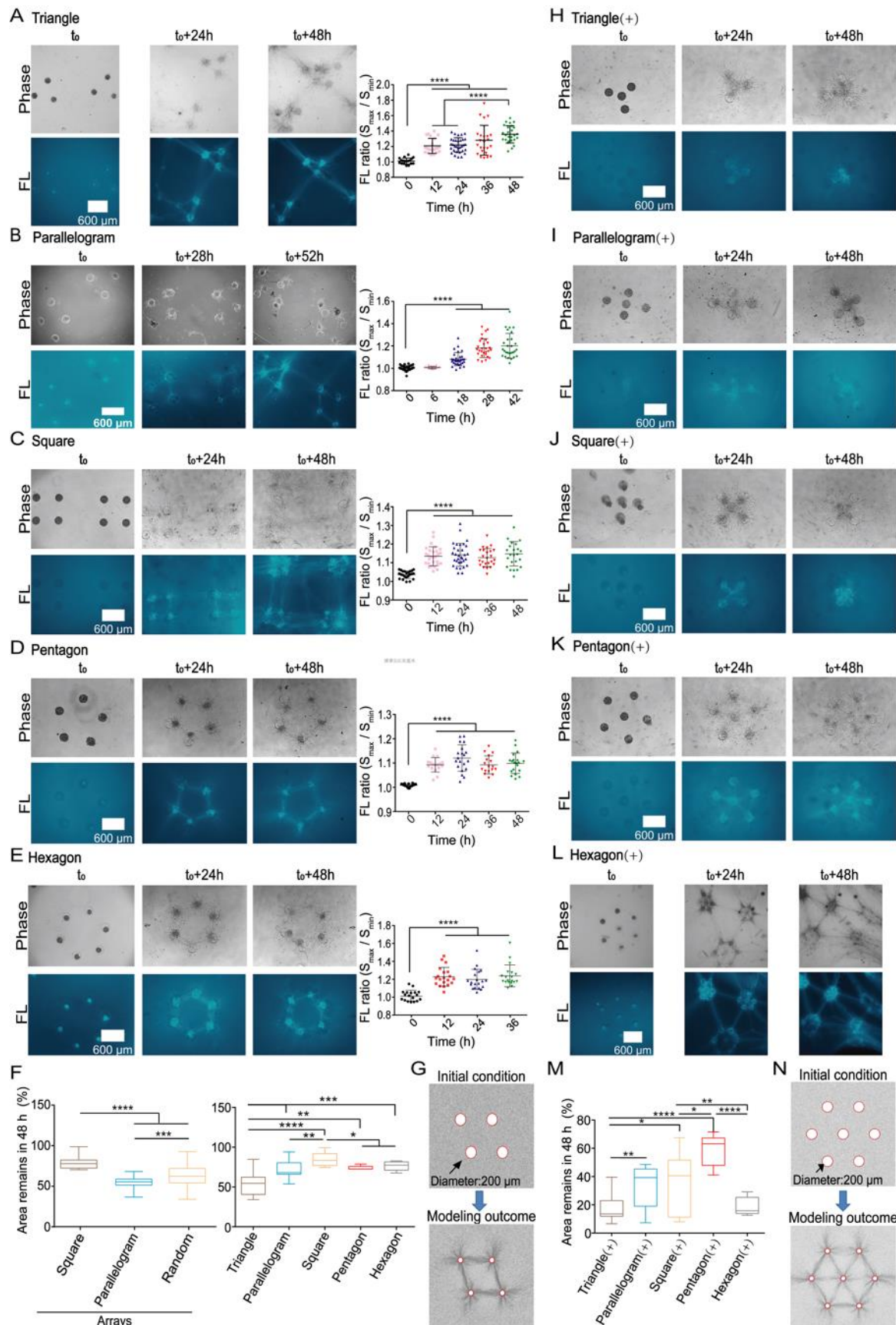
21

Figure 3. Fiber assembly in single polygons with diverse geometries, and their structural stabilities. Cell clusters were seeded into single polygons including triangles, parallelograms, squares, pentagons, and hexagons. In additional groups, there was a cell cluster positioned at the geometrical center of the polygons ('polygon(+)'). Images were acquired at the indicated time points in the next two days, and fluorescent COL fibers were measured as Ratio = S_{max}/S_{min}. **(A-E)** The growth of fluorescent COL fibers, and the fluorescence quantification (mean ± S.E.M.) for fiber strength in single triangles (**A**), parallelograms (**B**), squares (**C**), pentagons (**D**), and hexagons (**E**). **(F)** Stability measurements as remained areas (%) from geometrical shrinking for the diverse arrays (from Figure 2) and polygons within 48 h. The mean ± S.E.M. values for square array: 79.5±1.3; parallelogram array: 55.3±0.7; random array: 63.3±1.8; single triangle: 54.8±3.5; parallelogram: 71.6±2.6; square: 82.4±2.4; pentagon: 74.3±1.2; hexagon: 75.2±1.9. **(G)** The MD simulation for fiber clustering in a single parallelogram. **(H-L)** COL fiber growth and the structural stability in complexity-enhanced single polygon(+) including triangle(+) (**H**), parallelogram(+) (**I**), square(+) (**J**), pentagon(+) (**K**), and hexagon(+) (**L**). **(M)** Measurements of remained areas (%) for the diverse polygons(+) within 48 h. The mean ± S.E.M. values for triangle(+): 17.6±2.9; parallelogram(+): 32.7±3.9; square(+): 28.5±6.2; pentagon(+): 59.3±6.2; hexagon(+): 9.1±1.9. **(N)** The MD simulation for fiber clustering in a single hexagon(+).

The cytoskeleton integrity and actomyosin contraction are essential for remote induction of COL fiber assembly

Since cells induced fiber assembly in the experimental models, we further looked at the involved cellular biomechanical mechanism by applications of the large-spatial parallelogram arrays. First by checking the importance of cell cytoskeletons, at the control condition (with 0.1% DMSO in volume concentration), cells actively migrated out from clusters towards each other, and well

developed COL fiber networks (Fig. 4A); when actin cytoskeleton was inhibited with cytochalasin D (CytoD) or latruculin A (LatA) treatment, the fiber assembly was gone, and cells didn't migrate out actively (Fig. 4B, C); similar results were observed when microtubule cytoskeleton was inhibited with Nocodazole treatment (Fig. 4D). The representative images with more details for cytoskeleton inhibitions are presented in Figure S5(A-D). In this work, cell migration was just descriptive but not quantitative, as not the main focus of the study. The comparison of percentage changes based on COL fluorescence quantification showed inhibited fiber assembly by the three drug treatments (Fig. 4E). These data indicate that the integrity of both cellular actin and tubulin cytoskeletons are essential requirements for remote induction of the fiber assembly.

We continued to check the role of cellular actomyosin contraction which is mainly regulated by RhoA-ROCK-Myosin II signaling pathway[58]. In contrast to the control group with well-developed fiber network and active cell migrations (Fig. 4F), the induced fiber assembly disappeared after inhibition of ROCK with Y27632 (Fig. 4G). When inhibited actomyosin contraction with myosin ATPase inhibitor Blebbistanin, or myosin light-chain kinase inhibitor ML-7, fiber assembly was also blocked (Fig. 4H, I). The representative images with more details are presented in Figure S5(E-H). It is noted that after the contraction inhibitions, cell migrations were significantly reduced and shown in a scattering way but not directional (Fig. 4G-I), which is consistent with our recent work[23]. When inhibition of another small GTPase Rac1 with NSC23766 (40 μM), fiber assembly showed up with partial reductions, and cell migrations were less active (Figs. 4J, S5I). Similar results were observed while with more reduced cell migrations at higher concentration of NSC23766 (100 μM) (Fig. S5J). The comparisons from fluorescent fiber quantifications showed blocked fiber assembly after the contraction inhibitions, while partial

inhibition with Rac1 inhibitor (Fig. 4K). These data together indicate that actomyosin contractions from the cell clusters are essential for remote induction of COL fiber assembly.
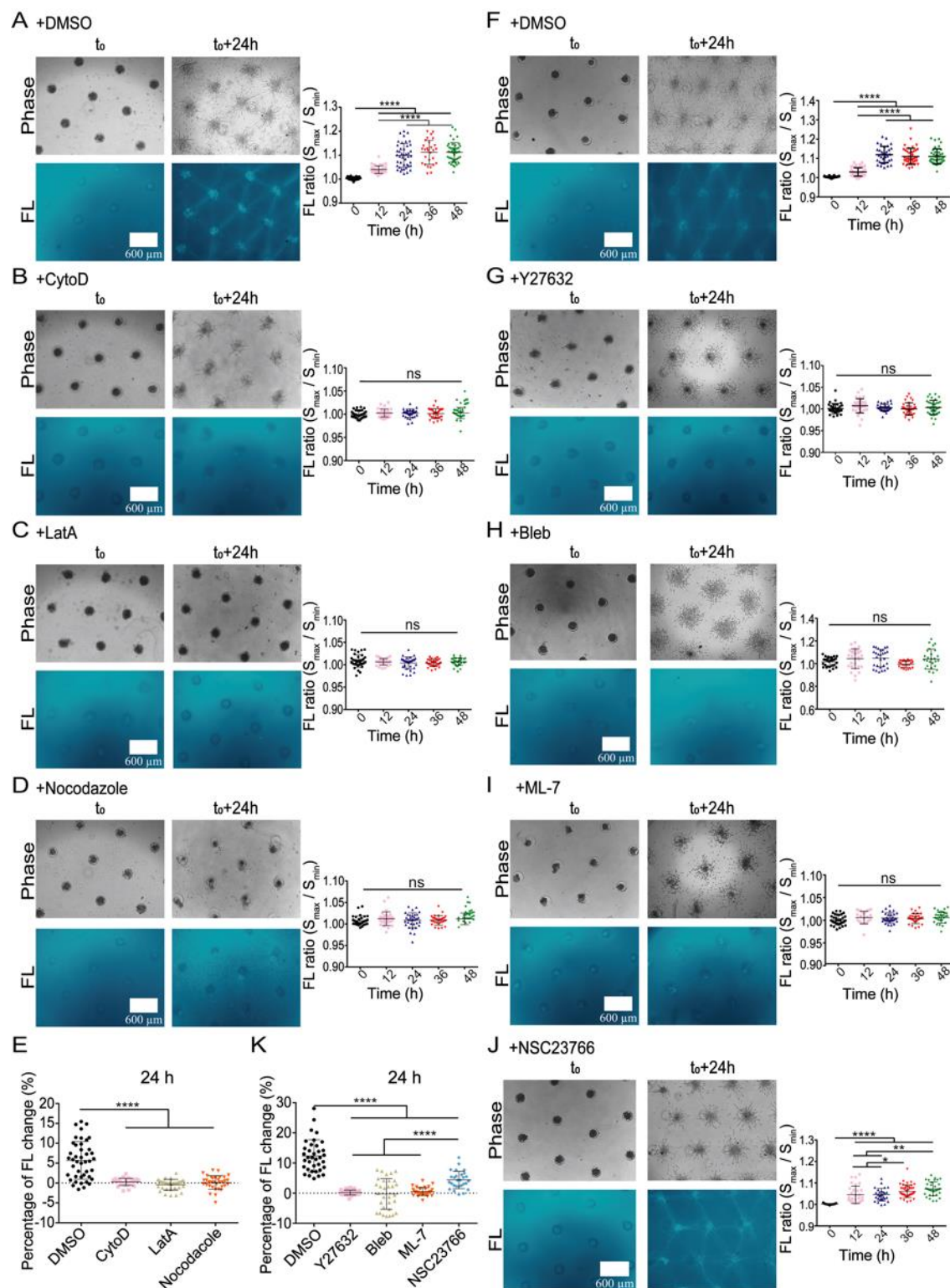
Figure 4. Cytoskeleton integrity and actomyosin contraction in remote induction of fiber assembly. Cell clusters were cultured into large parallelogram arrays with cytoskeleton or actomyosin inhibitors. **(A-D)** The COL fiber growth and fluorescence quantification at control condition (DMSO) (**A**), or under treatment with 1 µM CytoD (**B**), 237 nM LatA (**C**), or 1 µM Nocodazole (**D**). **(E)** Comparison for the percentage changes of COL fiber fluorescence within 24 h with or without cytoskeleton inhibitors. **(F-J)** The COL fiber growth and fluorescence quantifications at control condition (DMSO) (**F**), or under treatment with 40 µM Y27632 (**G**), 40 µM Blebbistanin (**H**), 40 µM ML-7 (**I**), or 40 µM NSC23766 (**J**). **(K)** Comparison for the percentage changes of COL fiber fluorescence within 24 h at the indicated conditions.

Calcium channels mediate cell clusters-induced fiber assembly

Our recent work showed that calcium channels at endoplasmic reticulum (ER) membrane are critical in cell-cell mechanical communications[23]. Here we further examined whether the importance in the remote induction of fiber assembly. Similarly, COL fibers were assembled into network structure in the parallelogram arrays along with active cell migrations under control condition (Fig. 5A). When inhibition of inositol 1,4,5-trisphosphate receptor (IP$_3$R) calcium channel or SERCA pump at the ER membrane with 2-APB or Thapsigargin, both fiber assembly and cell migrations were almost blocked (Fig. 5B, C). Inhibition of L-type calcium channel at the plasma membrane with Nifedipine also resulted into large inhibition of fiber assembly and cell migration (Fig. 5D), whereas inhibition of plasma membrane Store-operated calcium channels (SOCs) with LaCl$_3$ had little effect (Fig. 5E). The representative images with more details are shown in Fig. S6(A-E). The percentage increases in fiber fluorescence quantification confirmed

25

these observations (Fig. 5F). These results indicate that calcium signals regulated by the ER store and plasma membrane are important for cell clusters-induced fiber assembly.
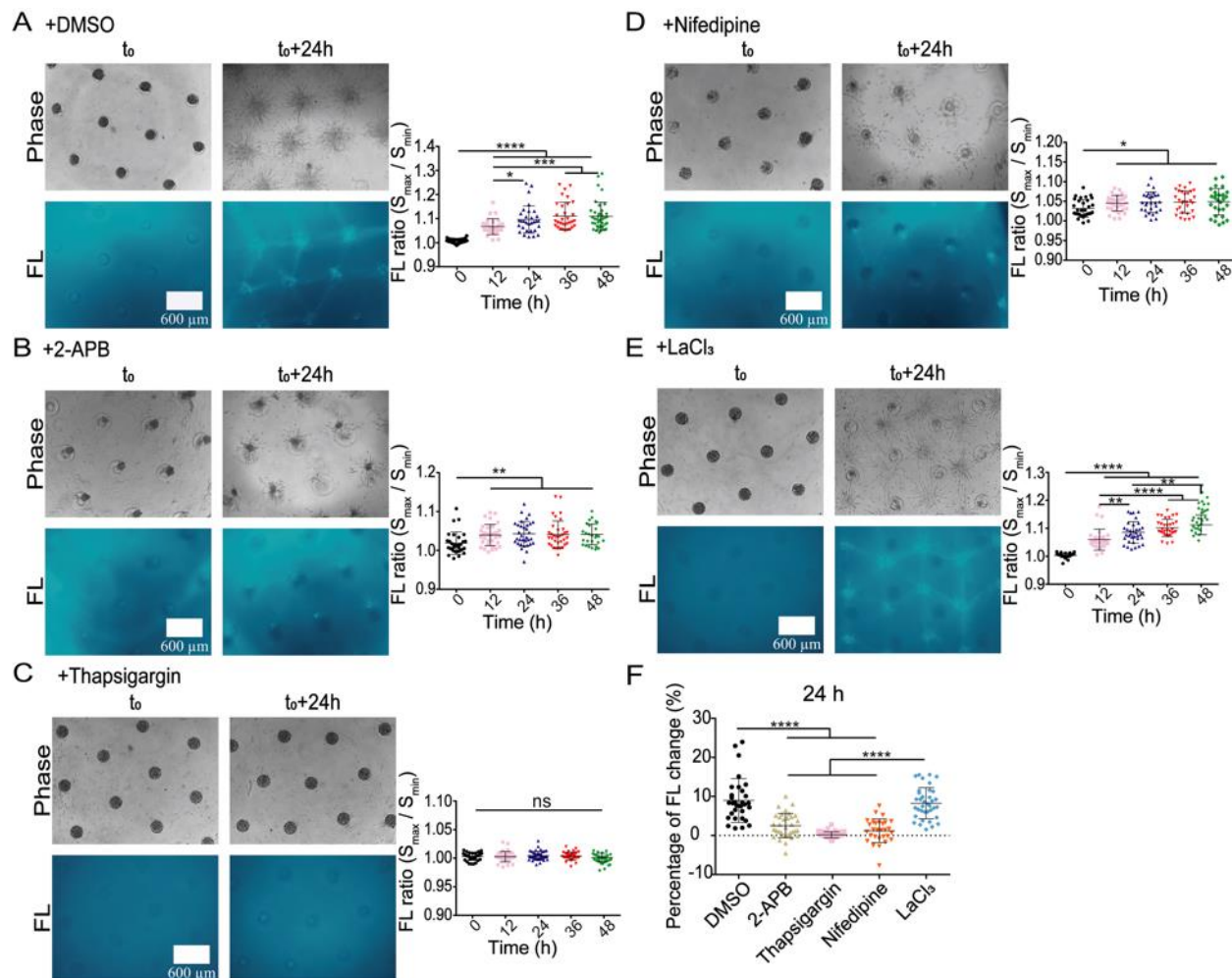

Figure 5. Calcium channels in regulating cell clusters-induced fiber assembly. Cell clusters were positioned into geometrical parallelogram arrays, and treated with or without calcium channel inhibitors. **(A-E)** Fiber assembly and fluorescence quantifications at control condition (DMSO) (**A**), or treated with 20 µM 2-APB (IP$_3$R channel inhibitor) (**B**), 10 µM Thapasigargin (SERCA pump inhibitor) (**C**), 20 µM Nifedipine (L-type channel inhibitor) (**D**), or 100 µM LaCl$_3$ (SOCs inhibitor) (**E**). **(F)** Comparison for fiber fluorescence changes (%) in 24 h under the indicated conditions.

26

The less criticalness of membrane mechanosensitive integrin β1 or Piezo1 alone in remote induction of fiber assembly

Plasma membrane integrin and Piezo1 are mechanosensitive components[21; 23]. Here, we examined their roles in the remote induction of COL fiber assembly. After down-regulation of integrin β1 expression with siRNA transfection in ASM cells, COL fibers were still induced apparently while cell migration was less active, in comparison to the control group without transfection or with control siRNA (Figs. 6A-C, S7A-C). Fluorescence quantification showed slight inhibition of fiber assembly with integrin β1 down-regulation (Fig. 6D&E). After inhibition of Piezo1 with siRNA transfection, there was little effect on the fiber assembly (Figs. 6F-H, S7D-F). Fiber fluorescence quantification didn't show inhibitory role when Piezo1 was inhibited (Fig. 6I&J). These data indicate that either of the two mechanosensitive molecules alone on the plasma membrane was less critical in remote induction of fiber assembly by cell clusters.
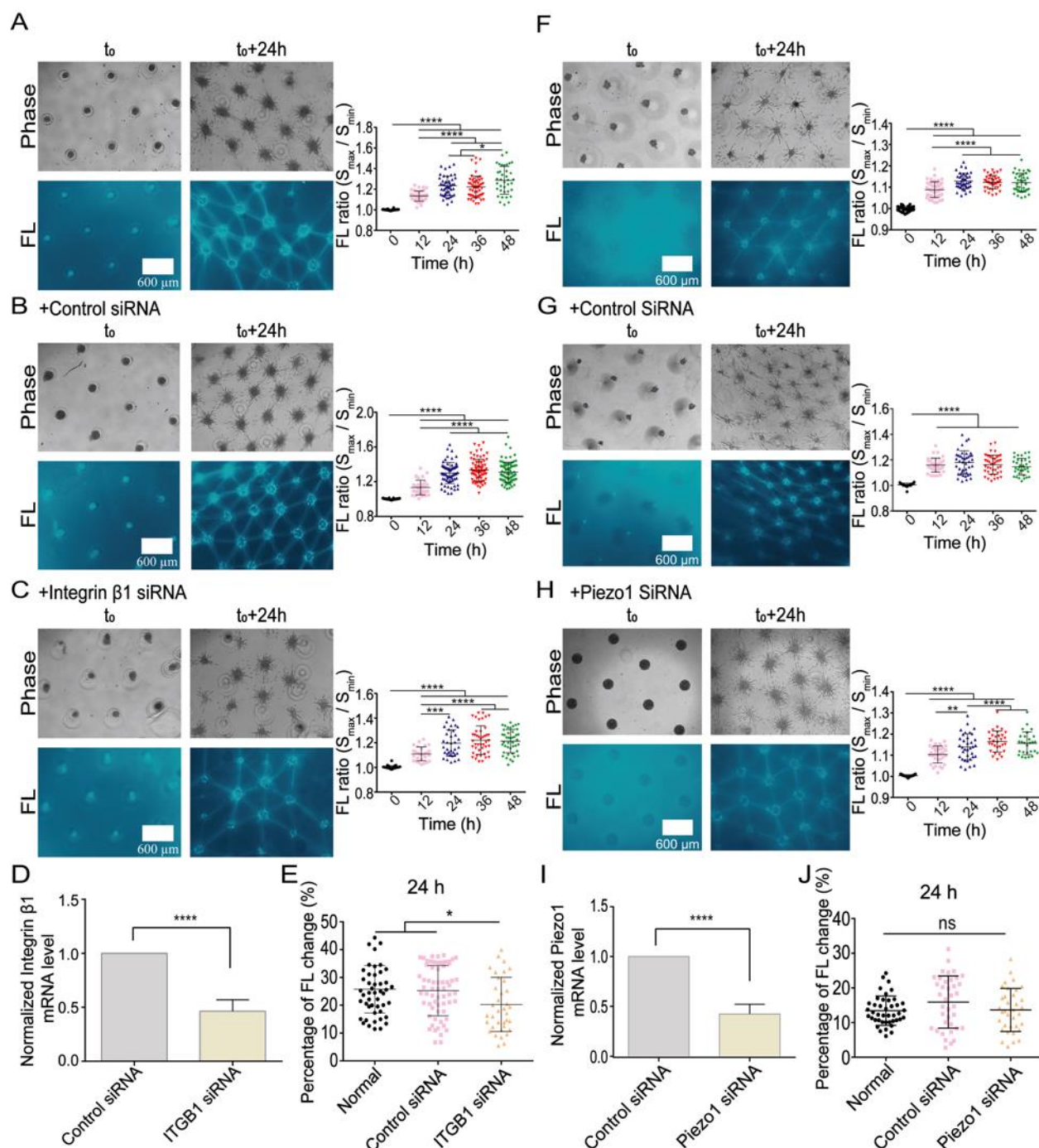
Figure 6. The role of integrin β1 and Piezo1 in fiber inductions. ASM cells were transfected with positive or negative siRNA (50 nM) for integrin β1 (ITGB1) or Piezo1. COL fiber inductions were recorded and quantified in experiments with geometrical parallelogram-arrayed cell clusters. **(A-C)** Fluorescent COL fibers and quantifications under the condition of cell clusters without

transfection (**A**), or with negative siRNA (**B**) or ITGB1 siRNA (**C**) transfection. **(D, E)** The mRNA expression levels (**D**) and comparison of percentage changes in fiber growth (**E**) under control or ITGB1 siRNA-transfected condition. **(F-H)** Fluorescent COL fibers and quantifications under the condition without transfection (**F**), or with negative siRNA (**G**) or Piezo1 siRNA transfection (**H**). **(I, J)** The mRNA expression levels (**I**) and percentage changes in fiber growth (**J**) in control groups or Piezo1 siRNA-transfected group.

Discussion

The long-range or large-spatial mechanical communications and resulted ECM modeling provide another angle in understanding physiological homeostasis in vivo, tissue morphogenesis, and the progressing in certain diseases. In this work, we tried to investigate the biophysical mechanism of large-spatial fiber assembly induced remotely by cells in COL hydrogel, and the supporting cell molecular mechanism. By incorporating dynamic contractions from cells, Molecular Dynamics (MD) along with Finite Element (FE) modeling was able to simulate large-scale COL fiber clustering under variable geometrical distributions of cells. Experimental outcomes based on designed distributions of cell clusters in arrays yielded similar results to the simulated ones, which also provided a platform in examining the involved cellular signals.

Large-spatial and dynamic simulations for remote COL fiber clustering by MD and FE modeling with cell experimental verifications

According to the previous observations that the cells-derived traction force was dynamic but not static in the hydrogels, MD simulation containing the dynamic factor was applied to model the COL fiber clustering induced remotely by cells (Fig. 1A-C). The simulated results were consistent

29

with the calibrated maximum shear stress distributions from FE modeling (Fig. 1D-I), which didn't have pre-conditional limitations like cell shape, cell number, geometry, or space. To check whether the simulated results occurred in reality, we designed experiments with variable geometrical arrays for cell cluster distributions (Fig. 2). The geometrically arranged cell clusters including large-spatial square, parallelogram, and random-style arrays were covered into a layer of fluorescent COL hydrogel. The three types of arrays yielded highly consistent results with the MD simulated ones under similar setups (Fig. 2). These data largely verified the MD simulations based on cell dynamic shear tractions, and also demonstrated the robustness of ECM modeling based on pre-designs.

COL fiber inductions in single polygons, and their contraction-associated structural stability

Beside the large-scale arrays, it is also interesting to examine the fiber inductions in single polygons with different geometries. It turned out that the appropriately seeded cell clusters produced triangles, squares, parallelograms, pentagons, and hexagons through COL fiber remodeling (Fig. 3A-E). Due to the assembly of the fiber scaffolds induced by cell contractions, their structural stability is also one interesting parameter. By measuring the area changes within 48 h culture, the large square array (~20% shrinkage) is more stable than parallelogram and random-style ones (~40-45% shrinking) (Fig. 3F, left graph). In single polygons, the squares are still the most stable (~18% shrinking), followed with pentagons and hexagons (~25% shrinking), then parallelograms (~30% shrinking) and triangles (~45% shrinking) (Fig. 3F, right graph). The stability of the assembled scaffolds can reflect the internal contraction strength and balance.

When introducing additional contraction with cell cluster at the geometrical center of the single polygons(+), the contraction balance within the assembled scaffolds was largely lost (~65-90% shrinking) except the pentagon(+) one (~40% shrinking) (Fig. 3H-M). This helps explain the cell

contractions-induced COL remodeling, and implicates the existence of tensions in maintaining the stability of the fiber structures. It is consistent with recent report that the fibers bear the major tensions between cells[29]. The MD simulations predicted the fiber clustering in the single parallelogram and hexagon(+) (Fig. 3G, N), but not yet the tension-mediated structural stabilities.

The cellular mechanical mechanism in mediating the remote inductions of fiber assembly

Inhibitions of cytoskeletons (actin microfilaments and microtubules) or myosin contractility blocked the fiber inductions (Fig. 4), which demonstrates cell contractions-dependent remodeling of COL hydrogel. It is noted that tubulin cytoskeleton, which doesn't provide cellular contraction force but gives mechanical supports, is also essential for the remote fiber inductions (Fig. 4D, E). Although there is no direct data to interpret this result yet, it may be related to microtubule functions in motility and intracellular transportations[59].

Calcium signal is mechanosensitive in cells[60; 61]. In this work, inhibitions of ER calcium channels IP$_3$R and SERCA pump, or plasma membrane L-type calcium channel largely reduced the capability of cell clusters in remote induction of fiber assembly (Fig. 5). Therefore, the physiological flow of Ca^{2+} between cells and the microenvironment, or between the cytoplasm and ER store is essential in driving the hydrogel remodeling. Besides other rich functions of calcium signals, in regarding the role of Ca^{2+} in regulating actomyosin contractility[62; 63], it can make certain connection for these mechanosensitive calcium channels in the fiber inductions.

Several studies have shown the importance for the membrane mechanosensitive integrin (β1) or Piezo1 in cell distant mechanical interactions[21; 22; 23]. Here, we further examined the role of the two components in cell remote induction of fiber assembly. By application of siRNA-transfection method, integrin β1 showed certain mediation on the induced fiber assembly (Fig. 6A-

31

F), whereas Piezo1 didn't display apparent effect (Fig. 6G-J). Since the remote fiber assembly is induced from contraction of cell clusters, integrin may show the role in mechanical transmission between cells and the surrounding hydrogel. Although cell migrations were not a major focus in this work, the cytoskeletons of microfilaments and microtubules seemed essential for cell movements in the experiments with different inhibitors (Fig. 4A-D), while myosin inhibitions led to reduced and non-directional migrations (Fig. 4F-J).

The prospective application for cultured scaffolds in tissue engineering

This work also yields one principal experience: to culture cells-induced scaffolds or tissue patterns according to pre-designs. Tissues and organs have their specific shapes or structures, which has been one intriguing topic in developmental biology, but also a challenge in tissue engineering. Here, based on inductions of COL hydrogel remodeling with pre-designed cell cluster distributions, we successfully produced square/parallelogram/random-array lattices with assembled fibers (Fig. 2), and also single polygonal structures from triangles to hexagons (Fig. 3), although their structural stabilities were variable. This may lead to a new pathway for micro-tissue bioengineering including neural network, skin tissue, microvascular system. Currently, tissue or organ engineering has been advanced from pre-manufactured artificial scaffolds including 3D bioprinting techniques[64; 65; 66; 67]. The experimental results from our work may provide an alternative method or a supplemental recipe in current field of tissue engineering and regenerative medicine.

Conclusions

In this work with incorporated dynamic tractions, the simulations with Molecular Dynamics yielded highly matching outcomes with the observed COL fiber bands from experiments based on large-spatial square, parallelogram and random-style arrays of cell clusters. The designed single

polygons with variable geometries led to well predicted structures with assembled COL fibers, which structural balance was not maintained when introducing additional contraction at the geometrical centers. The cell cytoskeletal integrity (actin filaments and microtubules), actomyosin contractions, and ER calcium channels were essential for the remote induction of COL fibers, whereas the role of membrane mechanosensitive integrin β1 or Piezo1 alone was less critical in fiber assembly. This work provided new mechanistic insights with dynamic and spatial factors on the remote induction of ECM modeling by cells, as well as the relevant cellular molecular mechanism. The assembled biomechanical scaffolds based on pre-designs may also lead to promising application in tissue engineering.

Author contributions: M.O. conceived the project, and M.O. and L.D. designed the research; B.B. and B.J. designed the computational programs and performed the stimulation work; Y.H. performed the majority of experiments; Y.H. and M.O. did the major data analysis & organization; W.C., H.L., and Y.J. helped with experiments and data analysis; L.D. provided the setups of equipment; M.O., Y.H., B.B., and L.D. prepared the paper.

Statement for No Conflict of Interest: All authors of this paper declare no conflict of interest in this work.

References

[1] A.I. Alford, K.M. Kozloff, and K.D. Hankenson, Extracellular matrix networks in bone remodeling. The international journal of biochemistry & cell biology 65 (2015) 20-31.

[2] H.K. Kleinman, D. Philp, and M.P. Hoffman, Role of the extracellular matrix in morphogenesis. Current opinion in biotechnology 14 (2003) 526-32.

[3] A.D. Theocharis, D. Manou, and N.K. Karamanos, The extracellular matrix as a multitasking player in disease. FEBS J 286 (2019) 2830-2869.

[4] B. Erdogan, M. Ao, L.M. White, A.L. Means, B.M. Brewer, L. Yang, M.K. Washington, C. Shi, O.E. Franco, A.M. Weaver, S.W. Hayward, D. Li, and D.J. Webb, Cancer-associated fibroblasts promote directional cancer cell migration by aligning fibronectin. J Cell Biol 216 (2017) 3799-3816.

[5] W. Han, S. Chen, W. Yuan, Q. Fan, J. Tian, X. Wang, L. Chen, X. Zhang, W. Wei, R. Liu, J. Qu, Y. Jiao, R.H. Austin, and L. Liu, Oriented collagen fibers direct tumor cell intravasation. Proceedings of the National Academy of Sciences of the United States of America 113 (2016) 11208-11213.

[6] D. Pankova, Y. Chen, M. Terajima, M.J. Schliekelman, B.N. Baird, M. Fahrenholtz, L. Sun, B.J. Gill, T.J. Vadakkan, M.P. Kim, Y.H. Ahn, J.D. Roybal, X. Liu, E.R. Parra Cuentas, J. Rodriguez, Wistuba, II, C.J. Creighton, D.L. Gibbons, J.M. Hicks, M.E. Dickinson, J.L. West, K.J. Grande-Allen, S.M. Hanash, M. Yamauchi, and J.M. Kurie, Cancer-Associated Fibroblasts Induce a Collagen Cross-link Switch in Tumor Stroma. Mol Cancer Res 14 (2016) 287-95.

[7] A.K. Harris, D. Stopak, and P. Wild, Fibroblast traction as a mechanism for collagen morphogenesis. Nature 290 (1981) 249-51.

[8] D. Stopak, and A.K. Harris, Connective tissue morphogenesis by fibroblast traction. I. Tissue culture observations. Dev Biol 90 (1982) 383-98.

[9] Y. Long, Y. Niu, K. Liang, and Y. Du, Mechanical communication in fibrosis progression. Trends Cell Biol 32 (2022) 70-90.

[10] F. Alisafaei, X. Chen, T. Leahy, P.A. Janmey, and V.B. Shenoy, Long-range mechanical signaling in biological systems. Soft matter 17 (2021) 241-253.

[11] C.A. Reinhart-King, M. Dembo, and D.A. Hammer, Cell-cell mechanical communication through compliant substrates. Biophysical journal 95 (2008) 6044-51.

[12] J.P. Winer, S. Oake, and P.A. Janmey, Non-linear elasticity of extracellular matrices enables contractile cells to communicate local position and orientation. PloS one 4 (2009) e6382.

[13] C.L. Guo, M. Ouyang, J.Y. Yu, J. Maslov, A. Price, and C.Y. Shen, Long-range mechanical force enables self-assembly of epithelial tubular patterns. Proceedings of the National Academy of Sciences of the United States of America 109 (2012) 5576-82.

[14] Q. Shi, R.P. Ghosh, H. Engelke, C.H. Rycroft, L. Cassereau, J.A. Sethian, V.M. Weaver, and J.T. Liphardt, Rapid disorganization of mechanically interacting systems of mammary acini. Proceedings of the National Academy of Sciences of the United States of America 111 (2014) 658-63.

[15] I. Nitsan, S. Drori, Y.E. Lewis, S. Cohen, and S. Tzlil, Mechanical communication in cardiac cell synchronized beating. Nat Phys 12 (2016) 472-+.

[16] L. Sapir, and S. Tzlil, Talking over the extracellular matrix: How do cells communicate mechanically? Semin Cell Dev Biol 71 (2017) 99-105.

[17] A. Shellard, A. Szabo, X. Trepat, and R. Mayor, Supracellular contraction at the rear of neural crest cell groups drives collective chemotaxis. Science 362 (2018) 339-343.

[18] A. Shellard, and R. Mayor, Collective durotaxis along a self-generated stiffness gradient in vivo. Nature 600 (2021) 690-694.

[19] M. Ouyang, Z. Qian, B. Bu, Y. Jin, J. Wang, Y. Zhu, L. Liu, Y. Pan, and L. Deng, Sensing Traction Force on the Matrix Induces Cell-Cell Distant Mechanical Communications for Self-Assembly. ACS biomaterials science & engineering 6 (2020) 5833-5848.

[20] H. Zarkoob, S. Chinnathambi, J.C. Selby, and E.A. Sander, Substrate deformations induce directed keratinocyte migration. J R Soc Interface 15 (2018).

[21] P. Pakshir, M. Alizadehgiashi, B. Wong, N.M. Coelho, X. Chen, Z. Gong, V.B. Shenoy, C.A. McCulloch, and B. Hinz, Dynamic fibroblast contractions attract remote macrophages in fibrillar collagen matrix. Nature communications 10 (2019) 1850.

[22] L. Liu, H. Yu, H. Zhao, Z. Wu, Y. Long, J. Zhang, X. Yan, Z. You, L. Zhou, T. Xia, Y. Shi, B. Xiao, Y. Wang, C. Huang, and Y. Du, Matrix-transmitted paratensile signaling enables myofibroblast-fibroblast cross talk in fibrosis expansion. Proceedings of the National Academy of Sciences of the United States of America 117 (2020) 10832-10838.

[23] M. Ouyang, Y. Zhu, J. Wang, Q. Zhang, Y. Hu, B. Bu, J. Guo, and L. Deng, Mechanical communication-associated cell directional migration and branching connections mediated by calcium channels, integrin beta1, and N-cadherin. Front Cell Dev Biol 10 (2022) 942058.

[24] K. Aoki, Y. Kondo, H. Naoki, T. Hiratsuka, R.E. Itoh, and M. Matsuda, Propagating Wave of ERK Activation Orients Collective Cell Migration. Developmental cell 43 (2017) 305-317 e5.

[25] R. Sunyer, V. Conte, J. Escribano, A. Elosegui-Artola, A. Labernadie, L. Valon, D. Navajas, J.M. Garcia-Aznar, J.J. Munoz, P. Roca-Cusachs, and X. Trepat, Collective cell durotaxis emerges from long-range intercellular force transmission. Science 353 (2016) 1157-61.

[26] R.S. Sopher, H. Tokash, S. Natan, M. Sharabi, O. Shelah, O. Tchaicheeyan, and A. Lesman, Nonlinear Elasticity of the ECM Fibers Facilitates Efficient Intercellular Communication. Biophysical journal 115 (2018) 1357-1370.

[27] X. Ma, M.E. Schickel, M.D. Stevenson, A.L. Sarang-Sieminski, K.J. Gooch, S.N. Ghadiali, and R.T. Hart, Fibers in the extracellular matrix enable long-range stress transmission between cells. Biophysical journal 104 (2013) 1410-8.

[28] L. Liang, C. Jones, S. Chen, B. Sun, and Y. Jiao, Heterogeneous force network in 3D cellularized collagen networks. Phys Biol 13 (2016) 066001.

[29] Q. Fan, Y. Zheng, X. Wang, R. Xie, Y. Ding, B. Wang, X. Yu, Y. Lu, L. Liu, Y. Li, M. Li, Y. Zhao, Y. Jiao, and F. Ye, Dynamically Re-Organized Collagen Fiber Bundles Transmit Mechanical Signals and Induce Strongly Correlated Cell Migration and Self-Organization. Angew Chem Int Ed Engl 60 (2021) 11858-11867.

[30] M.S. Rudnicki, H.A. Cirka, M. Aghvami, E.A. Sander, Q. Wen, and K.L. Billiar, Nonlinear strain stiffening is not sufficient to explain how far cells can feel on fibrous protein gels. Biophysical journal 105 (2013) 11-20.

[31] C. Barnes, L. Speroni, K.P. Quinn, M. Montevil, K. Saetzler, G. Bode-Animashaun, G. McKerr, I. Georgakoudi, C.S. Downes, C. Sonnenschein, C.V. Howard, and A.M. Soto, From single cells to tissues: interactions between the matrix and human breast cells in real time. PloS one 9 (2014) e93325.

[32] D. Stopak, N.K. Wessells, and A.K. Harris, Morphogenetic rearrangement of injected collagen in developing chicken limb buds. Proceedings of the National Academy of Sciences of the United States of America 82 (1985) 2804-8.

[33] R.K. Sawhney, and J. Howard, Slow local movements of collagen fibers by fibroblasts drive the rapid global self-organization of collagen gels. J Cell Biol 157 (2002) 1083-91.

[34] A.S. Abhilash, B.M. Baker, B. Trappmann, C.S. Chen, and V.B. Shenoy, Remodeling of fibrous extracellular matrices by contractile cells: predictions from discrete fiber network simulations. Biophysical journal 107 (2014) 1829-40.

[35] H. Wang, A.S. Abhilash, C.S. Chen, R.G. Wells, and V.B. Shenoy, Long-range force transmission in fibrous matrices enabled by tension-driven alignment of fibers. Biophysical journal 107 (2014) 2592-603.

[36] M.S. Hall, F. Alisafaei, E. Ban, X. Feng, C.Y. Hui, V.B. Shenoy, and M. Wu, Fibrous nonlinear elasticity enables positive mechanical feedback between cells and ECMs. Proceedings of the National Academy of Sciences of the United States of America 113 (2016) 14043-14048.

[37] Y.L. Han, P. Ronceray, G. Xu, A. Malandrino, R.D. Kamm, M. Lenz, C.P. Broedersz, and M. Guo, Cell contraction induces long-ranged stress stiffening in the extracellular matrix. Proceedings of the National Academy of Sciences of the United States of America 115 (2018) 4075-4080.

[38] B.M. Baker, B. Trappmann, W.Y. Wang, M.S. Sakar, I.L. Kim, V.B. Shenoy, J.A. Burdick, and C.S. Chen, Cell-mediated fibre recruitment drives extracellular matrix mechanosensing in engineered fibrillar microenvironments. Nature materials 14 (2015) 1262-8.

[39] C.D. Davidson, D.K.P. Jayco, W.Y. Wang, A. Shikanov, and B.M. Baker, Fiber Crimp Confers Matrix Mechanical Nonlinearity, Regulates Endothelial Cell Mechanosensing, and Promotes Microvascular Network Formation. Journal of biomechanical engineering 142 (2020).

[40] L. Cassereau, Y.A. Miroshnikova, G. Ou, J. Lakins, and V.M. Weaver, A 3D tension bioreactor platform to study the interplay between ECM stiffness and tumor phenotype. J Biotechnol 193 (2015) 66-9.

[41] Y. Wu, Z. Jiang, X. Zan, Y. Lin, and Q. Wang, Shear flow induced long-range ordering of rod-like viral nanoparticles within hydrogel. Colloids Surf B Biointerfaces 158 (2017) 620-626.

[42] X. Li, R. Balagam, T.F. He, P.P. Lee, O.A. Igoshin, and H. Levine, On the mechanism of long-range orientational order of fibroblasts. Proceedings of the National Academy of Sciences of the United States of America 114 (2017) 8974-8979.

[43] W.H. Jung, N. Yam, C.C. Chen, K. Elawad, B. Hu, and Y. Chen, Force-dependent extracellular matrix remodeling by early-stage cancer cells alters diffusion and induces carcinoma-associated fibroblasts. Biomaterials 234 (2020) 119756.

[44] M. Ouyang, J.Y. Yu, Y. Chen, L. Deng, and C.L. Guo, Cell-extracellular matrix interactions in the fluidic phase direct the topology and polarity of self-organized epithelial structures. Cell Prolif 54 (2021) e13014.

[45] J. Wang, J. Guo, B. Che, M. Ouyang, and L. Deng, Cell motion-coordinated fibrillar assembly of soluble collagen I to promote MDCK cell branching formation. Biochemical and biophysical research communications 524 (2020) 317-324.

[46] D.G. Brownfield, G. Venugopalan, A. Lo, H. Mori, K. Tanner, D.A. Fletcher, and M.J. Bissell, Patterned collagen fibers orient branching mammary epithelium through distinct signaling modules. Curr Biol 23 (2013) 703-9.

[47] M. Aghvami, V.H. Barocas, and E.A. Sander, Multiscale mechanical simulations of cell compacted collagen gels. Journal of biomechanical engineering 135 (2013) 71004.

[48] K. Tanner, H. Mori, R. Mroue, A. Bruni-Cardoso, and M.J. Bissell, Coherent angular motion in the establishment of multicellular architecture of glandular tissues. Proceedings of the National Academy of Sciences of the United States of America 109 (2012) 1973-8.

[49] Y. Duan, J. Long, J. Chen, X. Jiang, J. Zhu, Y. Jin, F. Lin, J. Zhong, R. Xu, L. Mao, and L. Deng, Overexpression of soluble ADAM33 promotes a hypercontractile phenotype of the airway smooth muscle cell in rat. Experimental cell research 349 (2016) 109-118.

[50] S.J. Aper, A.C. van Spreeuwel, M.C. van Turnhout, A.J. van der Linden, P.A. Pieters, N.L. van der Zon, S.L. de la Rambelje, C.V. Bouten, and M. Merkx, Colorful protein-based fluorescent probes for collagen imaging. PloS one 9 (2014) e114983.

[51] X. Fang, K. Ni, J. Guo, Y. Li, Y. Zhou, H. Sheng, B. Bu, M. Luo, M. Ouyang, and L. Deng, FRET Visualization of Cyclic Stretch-Activated ERK via Calcium Channels Mechanosensation While Not Integrin beta1 in Airway Smooth Muscle Cells. Front Cell Dev Biol 10 (2022) 847852.

[52] J. Wang, S. Zhao, L. Luo, Y. Liu, E. Li, Z. Zhu, and Z. Zhao, Shengjing Capsule Improves Spermatogenesis through Upregulating Integrin alpha6/beta1 in the NOA Rats. Evid Based Complement Alternat Med 2019 (2019) 8494567.

[53] K.I.K. Beca, B.M. Girard, T.J. Heppner, G.W. Hennig, G.M. Herrera, M.T. Nelson, and M.A. Vizzard, The Role of PIEZO1 in Urinary Bladder Function and Dysfunction in a Rodent Model of Cyclophosphamide-Induced Cystitis. Front Pain Res (Lausanne) 2 (2021) 748385.

[54] T. Ushiki, Collagen fibers, reticular fibers and elastic fibers. A comprehensive understanding from a morphological viewpoint. Arch Histol Cytol 65 (2002) 109-26.

[55] C.L. Wennberg, T. Murtola, S. Pall, M.J. Abraham, B. Hess, and E. Lindahl, Direct-Space Corrections Enable Fast and Accurate Lorentz-Berthelot Combination Rule Lennard-Jones Lattice Summation. J Chem Theory Comput 11 (2015) 5737-46.

[56] W. Humphrey, A. Dalke, and K. Schulten, VMD: visual molecular dynamics. J Mol Graph 14 (1996) 33-8, 27-8.

[57] S. He, C. Liu, X. Li, S. Ma, B. Huo, and B. Ji, Dissecting Collective Cell Behavior in Polarization and Alignment on Micropatterned Substrates. Biophysical journal 109 (2015) 489-500.

[58] M. Vicente-Manzanares, X. Ma, R.S. Adelstein, and A.R. Horwitz, Non-muscle myosin II takes centre stage in cell adhesion and migration. Nature reviews. Molecular cell biology 10 (2009) 778-90.

[59] C. Janke, and M.M. Magiera, The tubulin code and its role in controlling microtubule properties and functions. Nature reviews. Molecular cell biology 21 (2020) 307-326.

[60] T.J. Kim, C. Joo, J. Seong, R. Vafabakhsh, E.L. Botvinick, M.W. Berns, A.E. Palmer, N. Wang, T. Ha, E. Jakobsson, J. Sun, and Y. Wang, Distinct mechanisms regulating mechanical force-

induced Ca(2)(+) signals at the plasma membrane and the ER in human MSCs. Elife 4 (2015) e04876.

[61] T.J. Kim, J. Seong, M. Ouyang, J. Sun, S. Lu, J.P. Hong, N. Wang, and Y. Wang, Substrate rigidity regulates Ca2+ oscillation via RhoA pathway in stem cells. J Cell Physiol 218 (2009) 285-93.

[62] D.L. Allen, and L.A. Leinwand, Intracellular calcium and myosin isoform transitions. Calcineurin and calcium-calmodulin kinase pathways regulate preferential activation of the IIa myosin heavy chain promoter. The Journal of biological chemistry 277 (2002) 45323-30.

[63] C. Batters, D. Brack, H. Ellrich, B. Averbeck, and C. Veigel, Calcium can mobilize and activate myosin-VI. Proceedings of the National Academy of Sciences of the United States of America 113 (2016) E1162-9.

[64] S.V. Murphy, and A. Atala, 3D bioprinting of tissues and organs. Nature biotechnology 32 (2014) 773-85.

[65] A. Lee, A.R. Hudson, D.J. Shiwarski, J.W. Tashman, T.J. Hinton, S. Yerneni, J.M. Bliley, P.G. Campbell, and A.W. Feinberg, 3D bioprinting of collagen to rebuild components of the human heart. Science 365 (2019) 482-487.

[66] B. Grigoryan, S.J. Paulsen, D.C. Corbett, D.W. Sazer, C.L. Fortin, A.J. Zaita, P.T. Greenfield, N.J. Calafat, J.P. Gounley, A.H. Ta, F. Johansson, A. Randles, J.E. Rosenkrantz, J.D. Louis-Rosenberg, P.A. Galie, K.R. Stevens, and J.S. Miller, Multivascular networks and functional intravascular topologies within biocompatible hydrogels. Science 364 (2019) 458-464.

[67] Y.W. Ma, Hao; Wang, Qiqi; Cao, Xiaodong; Gao, Huichang, Piezoelectric conduit combined with multi-channel conductive scaffold for peripheral nerve regeneration. Chemical Engineering Journal 452 (2023).